Journal of Solid State Chemistry 184 (2011) 2381–2386

Contents lists available at ScienceDirect

Journal of Solid State Chemistry

journal homepage: www.elsevier.com/locate/jssc

Raman scattering from La-substituted $BiFeO_3$–$PbTiO_3$

K.K. Mishra, V. Sivasubramanian, R.M. Sarguna, T.R. Ravindran, A.K. Arora *

Condensed Matter Physics Division, Indira Gandhi Centre for Atomic Research, Kalpakkam 603 102, India

ARTICLE INFO

Article history:
Received 16 May 2011
Received in revised form
8 July 2011
Accepted 10 July 2011
Available online 19 July 2011

Keywords:
Raman spectroscopy
Mixed-crystals
Phase transition

ABSTRACT

Polycrystalline samples of pure $BiFeO_3$–$PbTiO_3$ (BF–PT) and those upon substituting Bi by La up to 50% ($x \leq 0.5$) were synthesized using a solid-state reaction method. A composition-driven tetragonal–cubic transition, identified from X-ray diffraction, was found to occur at $x=0.4$. We report the phonon spectra of pure and La-substituted BF–PT and its assignment. From the behavior of total Raman intensity, the origin of the symmetry-forbidden Raman spectra is identified to lie in substitutional disorder. The dependence of splitting of A_1–E modes and that of the LO–TO modes on composition are obtained and their consequences on ionicity are discussed.

1. Introduction

Multifunctional materials that couple electric, magnetic, and structural order parameters resulting in coexistence of ferroelectric, ferromagnetic, and ferroelastic behaviors have attracted considerable attention in recent years. There is a growing interest in complex ABO_3 type perovskite multiferroics, which exhibit magnetoelectric effect [1,2]. Such materials find applications in areas such as transducers, magnetic/ferroelectric data storage, spintronics, and magnetic sensors [3–6]. In this context, rhombohedral $BiFeO_3$ (BF) is unique among other multiferroic materials due to the coexistence of two types of long-range order: antiferromagnetic order below the Neel temperature $T_N=370$ °C and the ferroelectric order below the Curie temperature $T_C=827$ °C [7,8]. However, the compound was not found to show the magnetoelectric effect, as a spiral modulated spin structure led to disappearance of overall magnetization [9]. In addition, the electric polarization was also found to be quite low [10,11]. Furthermore, the synthesis of ideal perovskite phase of pure BF is difficult because of comparable thermodynamic stability of Fe^{3+} and Fe^{2+} states of iron in this compound [12,13].

In order to overcome these limitations, several solid-solutions have been synthesized and their properties are investigated. The solid-solutions of BF with other ABO_3 compounds such as $PbTiO_3$ (PT), $PrFeO_3$, and $BaTiO_3$ stabilize the perovskite phase and exhibit spontaneous magnetization [14–16]. Recently, Zhu et al. [17] have carried out structural studies on $(1-y)(BiFeO_3)$–$y(PbTiO_3)$ solid solutions as a function of composition. For $y \geq 0.31$, the system was found to become tetragonal (space group $P4mm$). Cheng et al. [18] studied La-modified BF–PT mixed-crystal system $0.45(Bi_{1-x}La_xFeO_3)$–$0.55(PbTiO_3)$ for $x \leq 0.3$ and found that remanent polarization and magnetization increased as a function of x. These single phase compounds were found to crystallize in the tetragonal perovskite structure (space group $P4mm$) similar to BF–PT. Recently, Singh et al. [19] have studied the $0.50(Bi_{1-x}La_xFeO_3)$–$0.50(PbTiO_3)$ for $x=0.5$ and found magnetoelectric coupling factor to be higher than that for pure $BiFeO_3$. Rietveld analysis of the data suggested a cubic structure for the solid-solution (space group $Pm3m$) [19]. These results suggest that this system should undergo a tetragonal–cubic structural transition in the range $0 \leq x \leq 0.5$. This has not been studied. Although there have been a large number of dielectric and magnetic studies on pure and La-substituted BF–PT demonstrating their excellent multiferroic properties [16–23], there is none on the phonon spectra of this family of compounds from a fundamental point of view. This in spite of the fact that the phonon dynamics can provide useful insight into microscopic properties such as mode softening, structure property relations, nature of local ordering, and structure in the nano-scale range [24,25]. Raman spectroscopy is a powerful technique for studying short-range order [26–28] and phase transitions in perovskites [26,29–31]. It may be pointed out that eight Raman-active phonons are expected for the tetragonal phase ($P4mm$), whereas for the cubic space group no first order Raman spectrum is expected. This is because all the atoms occupy sites with an inversion symmetry [26]. Here, we report synthesis and investigations of structural and vibrational properties of pure and La-substituted $(Bi_{1-x}La_x)_{0.5}Pb_{0.5}Fe_{0.5}Ti_{0.5}O_3$ compounds using X-ray diffraction and Raman spectroscopy. Polycrystalline powder samples were synthesized using solid-state reaction technique. The

* Corresponding author. Fax: +91 44 27480081.
E-mail address: aka@igcar.gov.in (A.K. Arora).

0022-4596/$ - see front matter © 2011 Elsevier Inc. All rights reserved.
doi:10.1016/j.jssc.2011.07.014

emphasis is to understand the nature of the phonons in this mixed-crystal system and to probe the crystallographic phase transition.

2. Experimental details

Polycrystalline $(Bi_{1-x}La_x)_{0.5}Pb_{0.5}Fe_{0.5}Ti_{0.5}O_3$ samples were synthesized for $x=0.0$, 0.2, 0.3, 0.4, and 0.5 by the solid-state reaction technique. High purity starting materials (Bi_2O_3, La_2O_3, PbO, Fe_2O_3, and TiO_2) of 99.9% purity (Alfa Aesar) weighed in stoichiometric proportion were mixed and ground together. Powders were then calcined in a closed platinum crucible for 3 h at 500 °C in air, reground and calcined again for 4 h at 800 °C. The calcined powders were pressed into pellets and sintered at 1100 °C for 2 h. Precaution was taken to avoid loss of PbO from the sample, which considerably affects the physical properties. This was done by placing $PbZrO_3$ powder around the pellet, which maintains a high partial pressure over the sample [32]. The pellet was about 10.5 mm in diameter and 1.5 mm thick.

X-ray powder diffraction patterns of the sintered samples were measured to determine the structure and confirm the phase purity. Cu-$K\alpha$ radiation was used for recording the diffraction patterns using Siemen's X-ray diffractometer (D500). Diffraction patterns were analyzed using STOE software for indexing the peaks and obtaining the refined lattice parameters. Raman spectra were recorded at ambient temperature using 514.5 nm line of an Ar-ion laser covering the range 40–1000 cm^{-1} using a Ranishaw micro-Raman spectrometer (model-InVia). A 100× objective was used for focussing the laser beam on the sample. The spectrometer resolution for 1800 l/mm grating was $\sim 2\ cm^{-1}$. For recording Raman spectra at low temperature, a Linkam stage was used along with a 20× objective. Data acquisition time and the laser power were adjusted for obtaining a good signal-to-noise ratio. The spectra were fitted to Lorenzian line shapes for obtaining the mode frequencies using PEAKFIT software (JANDEL). Energy dispersive X-ray (EDAX) analysis of the samples was carried out using Cam Scan (CS 3200) scanning electron microscope (SEM). For dielectric measurements, silver electrodes were applied on cleaned surfaces of the disk-shaped sintered pellets. Capacitance was measured using an impedance analyzer (Model N4L PSM 1735, Newton4th make) in the frequency range of 8–125 kHz.

3. Results and discussion

Fig. 1 shows X-ray diffraction patterns from the pure and La-substituted BF–PT ($0 \le x \le 0.5$). All the diffraction peaks could be fitted to the tetragonal phase with space group $P4mm$ for $x \le 0.3$. The tick pattern shown at the bottom of the figure is the calculated peak positions for the tetragonal phase for $x=0$. It may be pointed out that it is in principle possible to fit this pattern also to centrosymmetric space group $P4/mmm$. However, as BF–PT exhibits ferroelectric properties, it is more appropriate to analyze the structure under non-centrosymmetric space group $P4mm$. From the X-ray reflections, it can be seen that as there are no unindexed lines, the compounds are single phase. The (0 0 1) reflection at 20° 2θ is found to shift towards (1 0 0) peak and the two merge at $x=0.4$. This suggests a reduction in the c-cell parameter of tetragonal phase as x increases and attaining a value same as that of cell parameter a for $x=0.4$. Similar merging of doublets at $2\theta \sim 32°$, 47°, and 53° is also found corresponding to (1 0 1)–(1 1 0), (0 0 2)–(2 0 0), and (2 0 1)–(2 1 0) reflections, respectively. The c/a ratios were calculated to be 1.133, 1.047 and1.022 for $x=0.0$, 0.2, and 0.3, respectively. One can notice that the lattice anisotropy (c/a) becomes smaller with increasing

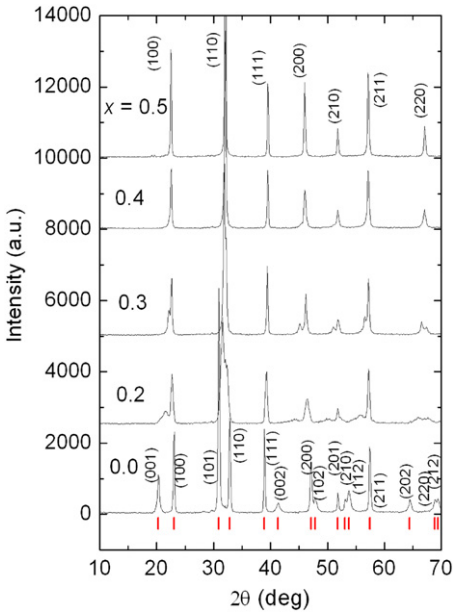

Fig. 1. X-rays diffraction patterns of $(Bi_{1-x}La_x)_{0.5}Pb_{0.5}Fe_{0.5}Ti_{0.5}O_3$ ($0 \le x \le 0.5$). The tick pattern is the calculated peak positions for the tetragonal phase ($P4mm$) for $x=0$.

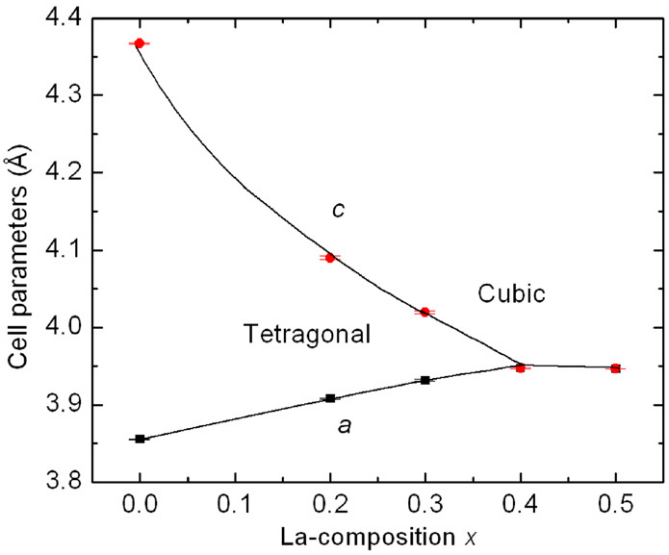

Fig. 2. Variation of the lattice parameters (c and a) as a function of composition in the La-substituted BF–PT solid solution system, ($0 \le x \le 0.5$). The curves drawn through the data are guide to the eye.

La-content. For $x \ge 0.4$, the diffraction patterns fit to a cubic structure with space group $Pm3m$. Thus, the structural change from tetragonal to cubic phase arises due to the homovalent substitution of Bi (ionic radius 1.34 Å) by La (ionic radius 1.36 Å) [33]. Fig. 2 shows the variation of the cell parameters as a function of La-composition. An unusually large tetragonality ($c/a=1.133$) is found for $x=0.0$, which decreases to 1.022 for $x=0.3$. For $x \ge 0.4$, the tetragonal distortion disappears and a cubic phase with lattice parameter $a=3.9467(2)$ Å emerges.

In order to study the chemical composition, EDAX was carried out on the samples. The EDAX spectrum for $x=0.5$, shown in Fig. 3, exhibits the presence of all the elements. The estimated compositions (final stoichiometry) were found to be in agreement with those of the starting compositions. The scanning electron

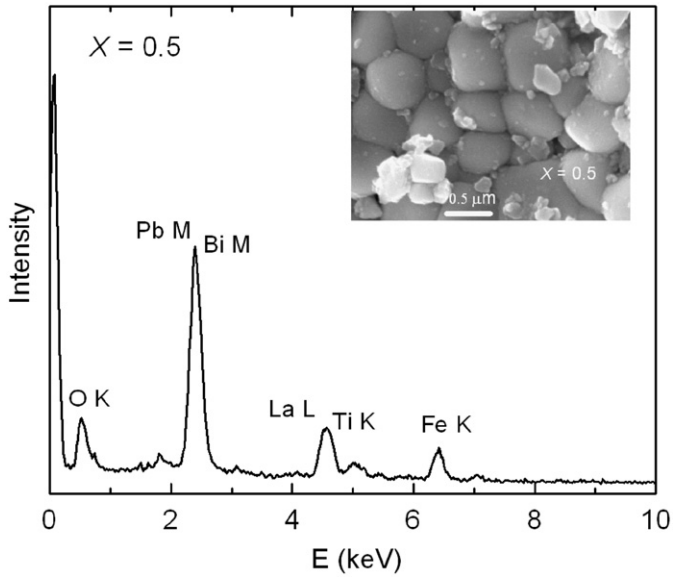

Fig. 3. EDAX spectrum of the sample for $x=0.5$. The inset shows SEM micrograph of fractured surface of the pellet.

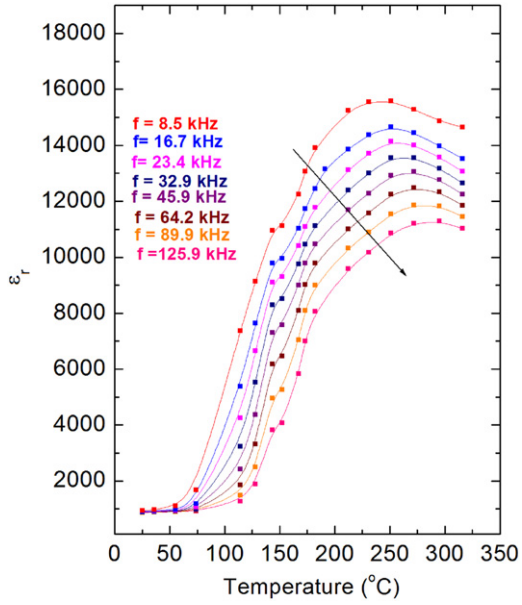

Fig. 4. Temperature dependence of real part of relative dielectric permittivity at various frequencies between 8 and 125 kHz for $x=0.5$. The arrow indicates the direction of increasing frequency.

micrograph (inset of Fig. 3) taken on a fractured surface for $x=0.5$ pellet reveals a well sintered nature of the pellet with an average grain size of 1–2 μm. Dielectric and magnetization measurements were also carried out on the samples. Fig. 4 shows ε_r vs T plot at different frequencies for $x=0.5$. It is evident that a diffuse (relaxor-type) phase transition is exhibited similar to that reported by others for 50% La-substituted BF–PT [19]. As the aim of the present study is to investigate the phonon spectra, the dielectric data is included briefly for the sake of completeness.

We now discuss the phonon spectra of BF–PT. As mentioned earlier, $PbTiO_3$ (PT) is a classical example of tetragonal ferroelectric material at ambient temperature and belongs to the space group $P4mm$. The irreducible representation of optical phonons in this phase is $\Gamma_{opt}=3A_1+4E+B_1$, where A_1 and E modes are both Raman and Infrared active, whereas the B_1 mode is only Raman

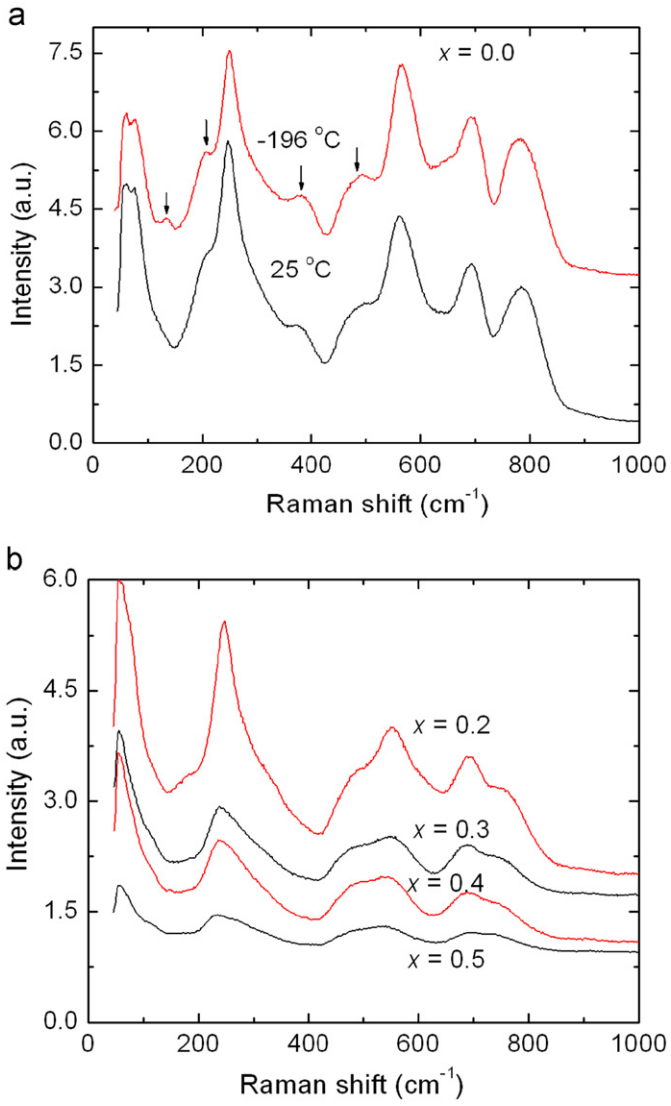

Fig. 5. (a) Raman spectra of $(Bi_{1-x}La_x)_{0.5}Pb_{0..5}Fe_{0.5}Ti_{0.5}O_3$ sample measured at 25 and −196 °C (For $x=0.0$), (b) Raman spectra of $(Bi_{1-x}La_x)_{0.5}Pb_{0.5}Fe_{0.5}Ti_{0.5}O_3$ samples ($0.2\le x\le 0.5$) at ambient.

active. Since BF–PT also has the same symmetry, the same set of modes is expected here too. Fig. 5 shows the Raman spectrum of pure BF–PT and also those of La-substituted compounds. Raman spectra of La-substituted BF–PT will be discussed later. In the case of pure BF–PT, five prominent peaks and three shoulders are discernible. By analyzing the spectra using PEAKFIT, ten modes could be identified in the frequency range 40–1000 cm^{-1}. The fitted mode frequencies are listed in Table 1 and are assigned by comparing with those of PT [34]. The lowest frequency mode appears at 65 cm^{-1}. In Raman spectrometers with a single monochromator and notch filter, often spectra are strongly attenuated at lower cm^{-1}. However, the notch filter used in this set up permits measurements down to 30 cm^{-1}. In order to confirm, whether the 65 cm^{-1} mode is genuine or an artifact of the notch filter, Raman spectrum of another compound $Zr(WO_4)_2$, which has a Raman peak at 41 cm^{-1}, was also recorded. The spectrum exhibited a clear mode at 41 cm^{-1}confirming the genuineness of the 65 cm^{-1} mode in BF–PT. One can see that none of the three A_1–LO modes are present; this may be either due to insufficient intensity or due to small LO–TO splitting of A_1 modes. All these modes are broad as compared to those reported [34] for $PbTiO_3$ single crystal. The broadening can arise due to

Table 1
Mode frequencies of the Raman bands in pure and La-substituted BF–PT for $x=0$ and 0.5 obtained from Lorenzian fitting of spectra. The reported mode frequencies of $PbTiO_3$ single crystal and their assignments are also included for comparision.

$(Bi_{1-x}La_x)_{0.5}Pb_{0.5}Fe_{0.5}Ti_{0.5}O_3$ present work mode frequency (cm^{-1})		Assignment	$PbTiO_3$[a] mode frequency (cm^{-1})
$x=0.0$	$x=0.5$		
65	63	$E^{(1)}$–TO	89
113	–	$E^{(1)}$–LO	130
199	–	$A_1^{(1)}$–TO	148
247	233	$E^{(2)}$–TO	220
284	276	$E^{(4)}$–TO, $E^{(4)}$–LO	290
380	–	$A_1^{(2)}$–TO	362
476	477	$E^{(2)}$–LO	440
566	540	$E^{(3)}$–TO	508
689	684	$A_1^{(3)}$–TO	650
789	733	$E^{(3)}$–LO	720

[a] Ref. [34].

several factors. The Raman spectrum of a polycrystalline powder sample is expected to be broader because of scattering of phonons at grain boundaries. In addition, because of randomly oriented grains, the phonon propagation direction is random with respect to crystallographic direction. Hence, the modes with mixed A_1–E character or mixed LO–TO character can arise. This is found even in polycrystalline powders and thin films of $PbTiO_3$ [35]. The broadening of spectrum can also arise due to finite (ambient) temperature of the sample, because phonon life-times are known to decrease as temperature is increased. In order to confirm whether the Raman bands become sharper upon lowering temperature, we have also measured the spectrum at $-196\,^{\circ}C$ and the same is included in Fig. 5(a). One can see that all the major peaks have nearly the same width while some of the weak bands that existed as shoulders such as those at 131, 199, 384 and 478 cm^{-1} (labeled with arrows), become more prominent at $-196\,^{\circ}C$. Thus, the temperature does not play a dominant role in determining the widths of the Raman bands in this mixed-crystal system. Another reason for phonon line-shape broadening could be the substitutional disorder arising from the random occupancy of cation site A by Bi/Pb and of cation site B by Fe/Ti. Consider a unit cell containing either FeO_6 or TiO_6 octahedron. Depending on the magnitude of the Fe–O and Ti–O force constants the bond distances can fluctuate from one unit cell to the other. This would make the characteristic vibrational frequencies of the two octahedra different. Although X-ray diffraction gives average cell parameters, and average atom positions for A, B, and O, on a microscopic scale there are fluctuations in the bond lengths and microscopic strains in the mixed-crystals [36]. Assuming that a given unit cell has TiO_6 octahedron, the six neighboring unit cells may have either TiO_6 or FeO_6 octahedra with a 50% probability. Thus, there are large number of ways in which different octahedral can occupy neighboring cells. Each of these configurations would result in slightly different vibrational frequencies and the total Raman lines shape. For example, for Ti–O stretching vibration, the spectrum will be a weighted sum of all possible frequencies. This argument is also valid for Bi–O and Pb–O vibrations. Thus, broadening of all modes is expected in 50–50 random solid-solution BF–PT as compared to pure PT. Raman spectra of La-substituted BF–PT, shown in Fig. 5(b), exhibit gradual change. For $x=0.2$ the Raman features are nearly the same except that the intensity is slightly reduced. For $x=0.3$, eight distinct Raman modes could be found in the same frequency range. The peaks are further broadened and the intensities reduced upon increasing the La-composition. Fig. 6 shows the individual components and total fitted spectrum for $x=0.4$.

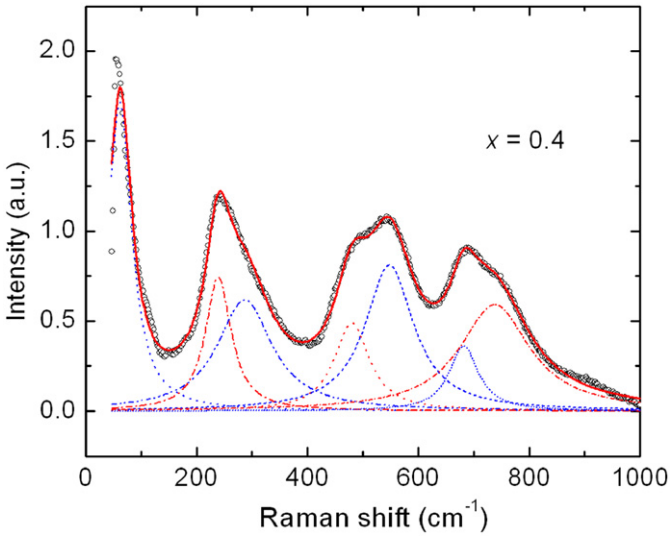

Fig. 6. Raman spectrum fitted to sum of 7 Lorenzian peaks for $x=0.4$ composition. Individual fitted peaks are also shown.

Table 2
Correlation diagram between irreducible representations of the C_{4v} (tetragonal) and O_h (cubic) point groups.

$(P4mm)\ C_{4v}$	$(Pm3m)\ O_h$
A_1 (R, IR)	F_{1u} (IR)
E (R, IR)	
B_1 (R)	F_{2u} (inactive)

Similar Lorenzian fitting has been done for other compositions also. Table 1 also lists the frequencies of observed Raman modes for $x=0.5$. In the cubic phase the fitting yielded seven modes. The modes in the cubic phase are even broader due to substitutional disorder. Substitutional disorder has been shown to cause a significant broadening of Raman line-shape in other mixed crystals [37].

As mentioned earlier, upon La-substitution the tetragonal anisotropy reduces and the system becomes cubic for $x \geq 0.4$. The irreducible representation for the optical phonons in the cubic phase is $\Gamma_{opt}=3F_{1u}+F_{2u}$, where the F_{1u} mode is Infrared active, and F_{2u} is a "silent mode", since it is inactive both in the Raman and in the infrared. These modes can be correlated to those of the tetragonal phase via a correlation diagram (Table 2). Thus, no Raman active modes are expected in the cubic phase. On the other hand, seven of the modes of the tetragonal phase for $x=0.3$ could be identified unambiguously in the cubic phase also. The modes in the cubic phase that have correspondence with those of the tetragonal structure appear to arise due to the breakdown of the Raman selection rule due to the substitutional disorder at the cation site and essentially represent the phonon density of states. Similar symmetry-forbidden Raman scattering has been reported in $BaTi_{1-x}Zr_xO_3$ and $BaCe_xZr_{1-x}O_3$ [30,31]. Very recently a small rhombohedral (space group $R3c$) distortion of the cubic phase has been reported, based on the presence of very weak satellite peaks in the neutron diffraction for $x=0.5$ system [38]. It may be pointed out that for the rhomohedral symmetry, a total of thirteen Raman active phonons ($4A_1+9E$) are expected [39]. On the other hand, in the present study we find only seven modes for $x \geq 0.4$. Furthermore, all these modes continue to have

correspondences with those of the tetragonal phase. In view of this, it is inappropriate to assign the modes of $x=0.4$ and 0.5 to those arising from a rhombohedral structure. In fact, the rhombohedral angle of the basic pseudo-cubic cell turns out to be 90.03° from the reported hexagonal primitive cell parameters [38]. It is likely that this small distortion is not able to activate the modes predicted for this symmetry. Thus, it is reasonable to attribute the spectra to symmetry-forbidden scattering.

In order to examine the manner in which total Raman intensity depends on the composition, we measured Raman spectra at large number of spots on each pellet and obtained the average integrated intensity (integrated from 40 to 1000 cm^{-1}). In order to make this intensity free from extrinsic factors such as laser power, focusing and alignment, a fused-quartz plate, placed next to the pellet, was also measured as a reference sample. Raman intensity from quartz plate was also integrated in the same spectral range. The total Raman intensity is shown in Fig. 7 after normalizing with that of the quartz. One can see that the scattered intensity decreases rapidly as x approaches tetragonal–cubic transition boundary. As the tetragonal distortion $(c/a-1)$ is only 0.022 at $x=0.3$, the Raman intensity has exhibited a large decrease as compared to lower x values. The fact that intensity does not become zero in the cubic phase implies that the symmetry-forbidden scattering is significant.

As the relaxor behavior in this system is well established [19], a discussion on the possible correlation of Raman spectra with the relaxor behavior is in order. Relaxor behavior arises due to existence of polar nano-grains (PNG) in randomly substituted mixed-crystal systems [26,40,41]. Microscopic compositional fluctuations or chemical ordering over a few nm length scale can give rise to formation of PNG although X-ray diffraction yields an average cubic structure consistent with the average stoichiometry. Within the PNG the local structure could be different due to the chemical ordering. As the Raman scattering is very sensitive to changes in local structure, sharp Raman peaks are sometimes [40,41] found, though not allowed by the cubic point group symmetry. In the present case, we do not find appearance of new sharp peaks riding over the symmetry forbidden broad spectrum. It is also worth examining if one can correlate/identify specific phonons with the magnetoelectric effect. In this context it is important to point out that ferroelectric

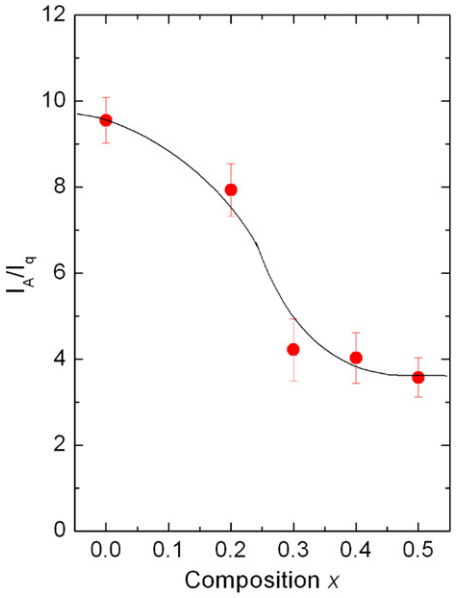

Fig. 7. Dependence of normalized integrated intensity on La-composition. Curve through the data is guide to the eye.

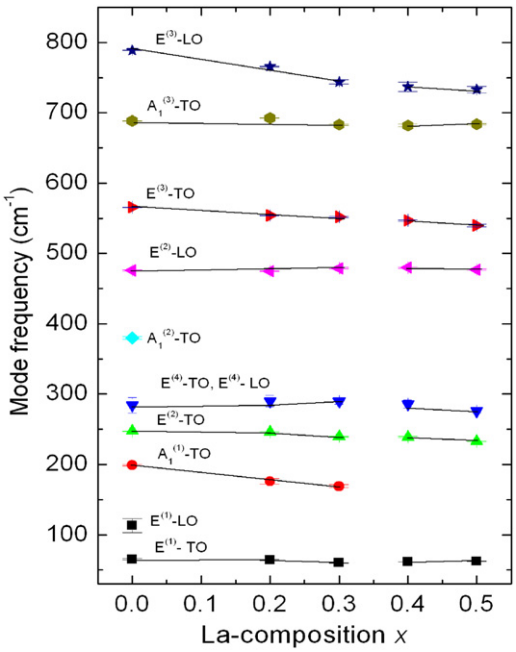

Fig. 8. Dependence of Raman mode frequency on La-composition. Lines through the data are guide to the eye.

and magnetic properties originate (a) in pure compounds from the equilibrium positions of different atoms in the unit cell and (b) in the substituted mixed-crystals from the displacements of atoms from ideal positions and/or formation of chemically ordered polar regions of nanometer length scale. Thus, optical phonons do not play direct role in determining the multiferroic properties. On the other hand, phonons do play an important role in inducing structural phase transitions and other physical properties.

The mode frequencies are shown as function of composition in Fig. 8. Some modes such as $A_1^{(1)}$–TO, $E^{(2)}$–TO, $E^{(3)}$–TO, $E^{(3)}$–LO show a decrease of the frequency as x increases, while a few other modes such as $E^{(1)}$–TO, $E^{(2)}$–LO, $A_1^{(3)}$–TO, etc. do not change significantly. It is worth examining the consequences of changes in the tetragonal distortion on the phonon spectra. As one can see from the correlation diagram, the triply degenerate F_{1u} mode of the cubic phase splits into a singly degenerate A_1 and a doubly degenerate E mode due to lowering of symmetry to tetragonal [34,42]. Thus, a reduction in the anisotropy splitting is expected as La-concentration is increased. Fig. 9 shows the separation of $A_1^{(1)}$–TO and $E^{(1)}$–TO as a function of tetragonal distortion c/a. Note that A_1–E anisotropy splitting reduces as c/a approaches unity. It may be pointed out that the $A_1^{(1)}$–TO and $E^{(1)}$–TO modes have been identified as the soft phonons in $PbTiO_3$ across tetragonal–cubic transition [34] at 495 °C. The softening of these phonons found in the present work as a function of La-composition is qualitatively similar to those of $PbTiO_3$. Fig. 9 also shows the LO–TO splitting of the $E^{(2)}$ mode as a function of c/a. This splitting is governed by Born's effective dynamic charges on the cations and anions. One can see that the LO–TO splitting increases upon La-substitution signifying an increase in the ionicity of the system.

4. Summary and conclusions

Pure and La-substituted $Bi_{1-x}La_xFeO_3$–$PbTiO_3$, polycrystalline samples were synthesized for compositions $x=0.0$, 0.2, 0.3, 0.4, and 0.5 by the solid-state reaction method. A single-phase perovskite structure was confirmed by X-ray diffraction. The system is found to exhibit a tetragonal–cubic structural transition

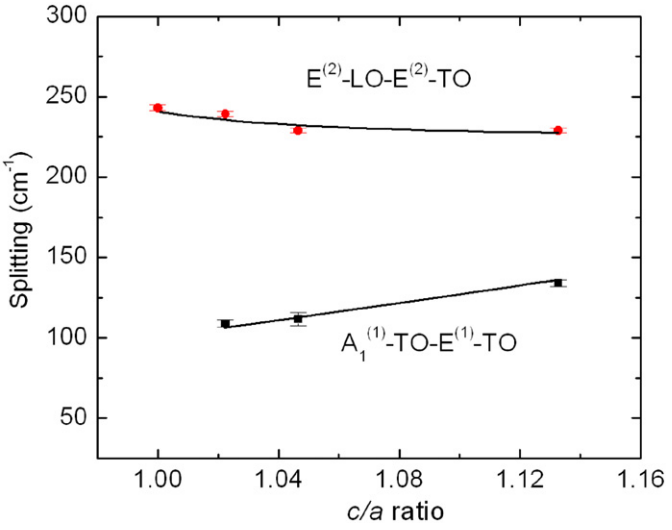

Fig. 9. Dependence of mode splitting on *c*/*a* ratio. Lines through the data are guide to the eye.

at $x=0.4$. In analogy with the tetragonal $PbTiO_3$, pure BF–PT also shows all the predicted Raman active vibrations. Although upon substituting Bi by La the intensities of the Raman modes are found to diminish, as many as seven modes are found in the cubic phase, which have correspondence with the modes of the tetragonal structure. These modes, although forbidden by the cubic point group symmetry, are activated by the substitutional disorder and represent phonon density of states. The decrease in the anisotropy splitting of the A_1 and E phonons is found to be consistent with the reduction in *c*/*a* ratio. The increase in LO–TO splitting upon increasing La-composition arises due to increased ionicity in the mixed-crystal system.

Acknowledgments

We acknowledge Mr. C.R. Das for EDAX analysis of the samples, Dr. V. Sridharan and Mr. Vijaya Kumbhar for dielectric measurements. We thank Dr. C.S. Sundar for interest in the work and Director IGCAR for encouragement.

References

[1] N.A. Hill, J. Phys. Chem. B 104 (2000) 6694.
[2] W. Eerenstein, N.D. Mathur, J.F. Scott, Nature 442 (2006) 759.
[3] G.A. Smolenskii, I. Chupis, Sov. Phys. Usp 25 (1982) 475.
[4] M. Fiebig, T. Lottermoser, D. Frohlich, A.V. Goltsev, R.V. Pisarev, Nature 419 (2002) 818.
[5] Y. Tokura, Science 312 (2006) 1481.
[6] J. Wang, J.B. Neaton, H. Zheng, V. Nagarajan, S.B. Ogale, B. Liu, D. Viehland, V. Vaithyanathan, D.G. Schlom, U.V. Waghmare, N.A. Spaldin, K.M. Rabe, M. Wutting, R. Ramesh, Science 299 (2003) 1719.
[7] Yu.N. Venevtsev, G. Zhdanov, S. Solov'ev, Sov. Phys. Crystallogr. 4 (1960) 538.
[8] G. Smolenskii, V. Isupov, A. Agranovskaya, N. Krainik, Sov. Phys. Solid State 2 (1961) 2651.
[9] F. Kubel, H. Schmid, Acta Crystallogr., Sect. B: Struct. Sci. 46 (1990) 698.
[10] M.M. Kumar, V.R. Palkar, K. Srinivas, V. Suryanarayana, Appl. Phys. Lett. 76 (2000) 2764.
[11] S.T. Zhang, M.H. Lu, D. Wu, Y.F. Chen, N.B. Ming, Appl. Phys. Lett. 87 (2005) 262907.
[12] X. Qi, J. Dho, R. Tomov, M.G. Blamire, J.L. MacManus-Driscoll, Appl. Phys. Lett. 86 (2005) 062903.
[13] W.M. Zhu, Z.-G. Ye, Ceram. Int. 30 (2004) 1435.
[14] V.V.S.S. Sai Sunder, A. Halliyal, A.M. Umarji, J. Mater. Res. 10 (1995) 1301.
[15] M.M. Kumar, A. Srinivas, S.V. Suryanarayana, T. Bhimasankaram, Phys. Status Solidi A 165 (1998) 317.
[16] K. Balamurugan, N.H. Kumar, P.N. Santhosh, J. Appl. Phys. 105 (2009) 07D909.
[17] W.-M. Zhu, H.-Y. Guo, Z.-G. Ye, Phys. Rev. B 78 (2008) 014401.
[18] J. Cheng, S. Yu, J. Chen, Z. Meng, Appl. Phys. Lett. 89 (2006) 122911.
[19] A. Singh, A. Gupta, R. Chatterjee, Appl. Phys. Lett. 93 (2008) 022902.
[20] W.-M. Zhu, Z.-G. Ye, Appl. Phys. Lett. 89 (2006) 232904.
[21] J.R. Cheng, L.E. Cross, J. Appl. Phys. 94 (2003) 5188.
[22] Y. Hadas, A. Sayapin, Y.E. Krasik, V. Bernshtam, I. Schnitzer, J. Appl. Phys. 104 (2008) 064125.
[23] T. Leist, T. Granzow, W. Jo, J. Rodel, J. Appl. Phys. 108 (2010) 014103.
[24] S.M. Cho, H.M. Jang, Appl. Phys. Lett. 76 (2000) 3014.
[25] M.N. Iliev, A.P. Litvinchuk, H.-G. Lee, C.L. Chen, M.L. Dezaneti, C.W. Chu, V.G. Ivanov, M.V. Abrashev, V.N. Popov, Phys. Rev. B 59 (1999) 364.
[26] N.K. Karan, R.S. Katiyar, T. Maiti, R. Guo, A.S. Bhalla, J. Raman Spectrosc. 40 (2009) 370.
[27] J. Frantti, V. Lantto, Phys. Rev. B 56 (1997) 221.
[28] J. Frantti, V. Lantto, J. Lappalainen, J. Appl. Phys. 79 (1996) 1065.
[29] H. Zhang, S. Leppavuori, P. Karjalainen, J. Appl. Phys. 77 (1995) 2691.
[30] P.S. Dobal, A. Dixit, R.S. Katiyar, J. Appl. Phys. 89 (2001) 8085.
[31] C. Chemarin, N. Rosman, T. Pagnier, G. Lucazeau, J. Solid State Chem. 149 (2000) 298.
[32] V. Sivasubramanian, V.R.K. Murty, B. Viswanathan, M. Sieskind, J. Phys.: Condens. Matter 8 (1996) 2447.
[33] R.E. Eitel, C.A. Randall, T.R. Shrout, P.W. Rehrig, W. Hackenberger, S.-E. Park, Jpn. J. Appl. Phys. 40 (2001) 5999.
[34] M.D. Fontana, H. Idrissi, G.E. Kugel, K. Wojcik, J. Phys.: Condens. Matter 3 (1991) 8695.
[35] D.S. Fu, H. Iwazaki, H. Suzuki, K. Ishikawa, J. Phys.: Condens. Matter 12 (2000) 399.
[36] O. Pages, A.V. Postnikov, M. Kassem, A. Chafi, A. Nassour, S. Doyen, Phys. Rev. B 77 (2008) 125208.
[37] S. Sahoo, S. Dhara, V. Sivasubramanian, S. Kalavati, A.K. Arora, J. Raman Spectrosc 40 (2009) 1050.
[38] A. Singh, R. Chatterjee, S.K. Mishra, P.S.R. Krishna, S.L. Chaplot, arxiv:1002.1545.
[39] R. Palai, H. Schmid, J.F. Scott, R.S. Katiyar, Phys. Rev. B 81 (2010) 064110.
[40] R. Martinez, R. Palai, H. Huhtinen, J. Liu, J.F. Scott, R.S. Katiyar, Phys. Rev. B 82 (2010) 134104.
[41] R. Ranjan, R. Hackl, A. Chandra, E. Schmidbauer, D. Trots, H. Boysen, Phys. Rev. B 76 (2007) 224109.
[42] R. Ouillon, J.-P. Pinan-Lucarre, P. Ranson, Ph. Pruzan, S.K. Mishra, R. Ranjan, D. Pandey, J. Phys.: Condens. Matter 14 (2002) 2079.